Applied Catalysis B: Environmental 182 (2016) 220–228

Contents lists available at ScienceDirect

Applied Catalysis B: Environmental

journal homepage: www.elsevier.com/locate/apcatb

Photocatalytic overall water splitting promoted by SnO_x–$NiGa_2O_4$ photocatalysts

Xiao-Jun Lv[a,*], Shixiong Zhou[b], Xing Huang[a], Chuanjun Wang[a], Wen-Fu Fu[a,b,**]

[a] Key Laboratory of Photochemical Conversion and Optoelectronic Materials and HKU-CAS Joint Laboratory on New Materials, Technical Institute of Physics and Chemistry, Chinese Academy of Sciences, Beijing 100190, PR China
[b] College of Chemistry and Chemical Engineering, Yunnan Normal University, Kunming 650092, PR China

ARTICLE INFO

Article history:
Received 7 July 2015
Received in revised form
10 September 2015
Accepted 15 September 2015
Available online 16 September 2015

Keywords:
High activity
Overall water splitting
Surface modification
Effective charge separation
Mechanism analysis

ABSTRACT

Overall water splitting is a huge challenge for the semiconductor photocatalysts. Herein, we investigated the high effective photocatalytic overall water stoichiometrically splitting into H_2 and O_2 activity using the SnO_x–$NiGa_2O_4$ (SNG) composites photocatalysts. Because of the effective charge separation and transfer in SnO_x–$NiGa_2O_4$ composites, the photocatalytic activity of the optimized composites photocatalysts can reach up to more than one order of magnitude greater than that of $NiGa_2O_4$ (NGO) or SnO_x alone respectively. In addition, under visible light irradiation the photocatalysts also displayed well both photocatalytic hydrogen evolution and pollution degradation potentials. More importantly, we further elucidated the essential band gap relation between the SnO_x and $NiGa_2O_4$ in the heterostructure, and a deep understanding of the charge separation mechanism based on the band alignment in such system was provided. Our study demonstrates great potential of the SnO_x–$NiGa_2O_4$ composites to be an attractive photocatalysts for the overall water splitting or pollution degradation under visible light irradiation.

1. Introduction

Direct overall water splitting to form hydrogen and oxygen using solar energy is one of the highly promising means for renewable energy production [1–7]. Tremendous efforts have been extensively directed toward the overall photocatalytic water splitting process with semiconductor based photocatalysts [3,8–14]. Nonetheless, this approach still suffers from some challenges that restrict the activity of overall water splitting for most of the semiconductor photocatalysts [15,16]. Generally, the rapid electron–hole recombination upon photo-excitation is one of the key issues for low photocatalytic efficiency of most of semiconductors, which varies depending on the intrinsic electronic and structural properties [14,15]. Therefore, effectively means of enhancing the charge separation efficiency of these photocatalysts is highly desirable and still endeavored. Many metal component as the cocatalyst can trap the photoexcited charge carriers and consequently promote the charge separation [17–19]. However, the most active and stable cocatalysts are still the noble metals such as Pt, Pd, Ru and Rh etc, which provide active sites and suppress the reformation of water and back electron transfer processes. Nevertheless, noble metals possess the disadvantages of being rare, expensive and harmful to the environment, which limits their wide application.

Surface modification of a photocatalyst combing two semiconductors of different electron affinity and ionization potentials [13,20–27] or different α–β phase junction on the same semiconductor [15] have been demonstrated to be effective methods to promote the charge separation and photocatalytic activity. For example, TiO_2 surface modified with Fe_2O_3 nanoparticles has shown visible light absorbance due to the presence of iron oxide particles on the surface, and enhanced the photocatalytic activity attributable to improved charge separation [28]. Other semiconductor based heterostructure photocatalysts such as CeO_2–TiO_2 [20], TiO_2–ZnO [17,29–31], SnO_2–TiO_2 [32,33], and Bi_2O_3–ZnO [22] etc. have also been demonstrated that the composites can effectively promote the catalytic activity due to increase in the rate of charge separation and reduction in the electron–hole pair recombination. Herein, we report surface modification of $NiGa_2O_4$ with SnO_x species and the formed composites can stoichiometrically split pure water into H_2 and O_2 with drastically enhanced photocatalytic activity compared to that with alone $NiGa_2O_4$ or SnO_x photocatalyst. The enhanced photocatalytic performance is attributed to the efficient charge separation and transfer between

* Corresponding author. Fax: +86 1082543520.
** Corresponding author at: Technical Institute of Physics and Chemistry, Chinese Academy of Science, Beijing 100190, PR China
E-mail addresses: xjlv@mail.ipc.ac.cn (X.-J. Lv), fuwf@mail.ipc.ac.cn (W.-F. Fu).

http://dx.doi.org/10.1016/j.apcatb.2015.09.032
0926-3373/

Table 1
Physical Properties of the SnO_x–$NiGa_2O_4$–y composite photocatalysts.

Sample	Tin concentration /mmol L^{-1} 0.1 N HCl (y)	Surface area/m^2 g^{-1}	Expected[a]	Measured bulk[b]	Measured surface[c]
			Sn/(Sn + Ni + Ga)	Sn/(Sn + Ni + Ga)	Sn/(Sn + Ni + Ga)
$NiGa_2O_4$	0	80	0	0	0
SNG 2	20	76	0.24	0.25	0.25
SNG 4	40	85	0.39	0.32	0.40
SNG 8	80	90	0.56	0.40	0.48
SNG 12	120	83	0.66	0.51	0.62
SNG 16	160	70	0.72	0.58	0.73
SNG 20	200	65	0.76	0.65	0.82

[a] Metal molar ratio in the synthesis solution.
[b] From SEM-EDX measurements at low magnifications.
[c] From XPS measurements.

two semiconductors. Tin is inexpensive, nontoxic and abundant, SnO_x has been demonstrated that show exceptionally higher photocatalytic activity compared to SnO_2, which is ascribed to the incorporation of Sn^{2+} into the lattice matrix of SnO_2 and accompanying oxygen vacancies, resulting in narrowing of the band gap and efficient separation of the photoexcited electron–hole pairs [34,35]. Furthermore, modification of a d10 semiconductor oxide ($ZnGa_2O_4$) with SnO_x as surface species have been demonstrated to lead to visible light absorbance behavior of the semiconductor material, which originated from the presence of Sn^{2+} (5 s) orbitals. Meanwhile, the practice results in a simultaneous effective separation of charges and holes and an increase in the photo-oxidative reactivity of holes for the degradation organic dye under the UV and visible irradiation [36].

$NiGa_2O_4$ is a semiconductor material in spinels crystallization form, and was found to be a potential catalyst for the NO reduction as well as for the photocatalytic dissociation of water [37–39]. The hollow rods of nanocrystalline $NiGa_2O_4$ was prepared using Ga_2O_3 and nickel salt and demonstrated high photocatalytic hydrogen evolution activity [38]. And we have reported the pH dependent preparation of octahedral $NiGa_2O_4$ with highly reactive facets by a hydrothermal method without using any template or organic solvent. In the presence of 1% RuO_2 as co-catalyst and methanol as sacrificial reagent, the octahedral $NiGa_2O_4$ displayed dramatic photocatalytic hydrogen generation activity from water [40]. However, the limitation of rapid recombination of electrons and holes still need to be handled to enhance the overall photocatalytic water splitting activity of $NiGa_2O_4$. Herein, we initially report the preparation of SnO_x–$NiGa_2O_4$ composite materials with SnO_x as the surface species and their application in overall photocatalytic water splitting. The prepared SnO_x–$NiGa_2O_4$ demonstrated better photocatalytic overall water splitting activity compared to a series of other photocatalysts, such as SnO_x–$ZnGa_2O_4$, SnO_x–$ZnGe_2O_4$, $NiGa_2O_4$, SnO_x, or TiO_2 (P25). Moreover, the essential band gap relationship between the heterostructure semiconductors was elucidated and the mechanism of effective charge separation based on the band alignment in such system was also studied in depth, which would be useful to provide some insight in the design and preparation of efficient semiconductor based photocatalysts.

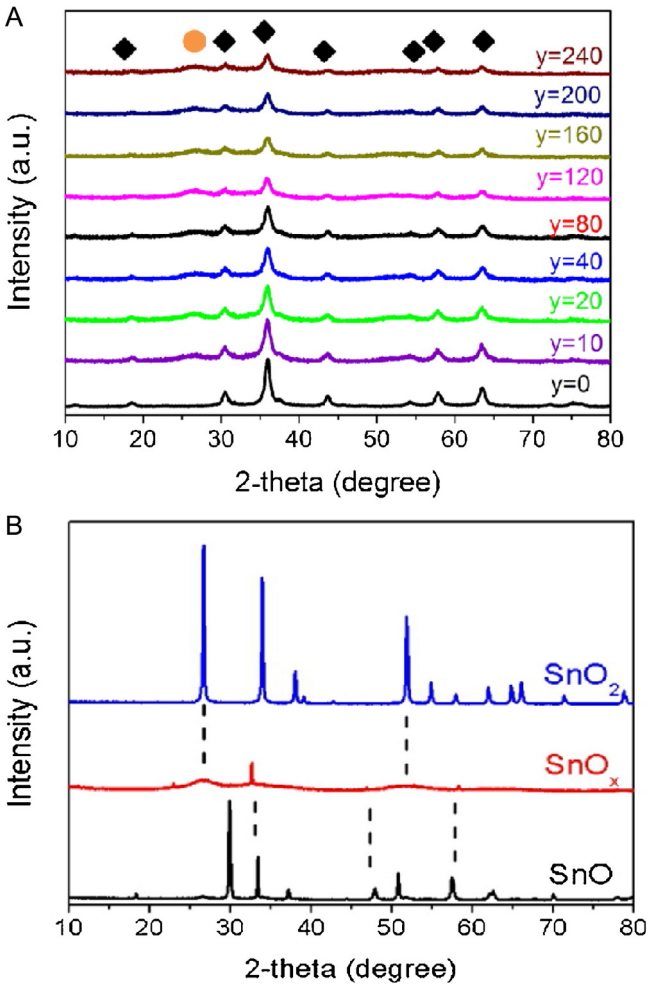

Fig. 1. XRD for (A) different SnO_x content in SnO_x–$NiGa_2O4$ photocatalyst. (♦): $NiGa_2O4$, (●): SnO_x; (B) the XRD patterns for SnO, SnO_x and SnO_2.

2. Experimental

2.1. Preparation of samples

All chemicals were analytical purity and used as received without further purification. The $NiGa_2O_4$ photocatalyst samples were prepared *via* a modified ion-exchange method [41]. $NaGaO_2$ precursor was firstly prepared by calcining the mixture of Ga_2O_3 and Na_2CO_3 (molar ratio of 1:1) at 700 °C for 6 h, the resultant white solid was milled into powder and heated at 900 °C for another 10 h. The $NaGaO_2$ suspension (0.2 mol L^{-1}, 10 mL) was added to an aqueous solution of $Ni(CH_3COO)_2$ (0.05 mol L^{-1}, 20 mL) and stirred for 1 h at room temperature. pH was adjusted using HCl (1 mol L^{-1}) or NaOH (1 mol L^{-1}) solution from 4 to 13, and stirred for 1 h. The obtained suspension solution was transferred into a Teflon-lined autoclave and thermally treated at 180 °C for 15 h. The obtained precipitate was washed with hydrochloric acid (0.1 mol L^{-1}) and distilled water several times, respectively. The obtained precipitate subsequently dried in an oven at 70 °C over night.

SNG composites were synthesized according to the modified hydrothermal method [36]. Initially, 0.25 g of $NiGa_2O_4$ was stirred in an ethanol solution (20 mL ethanol + 10 mL water). This was transferred to a solution of tin chloride in 46 mL of 0.1 M HCl (dif-

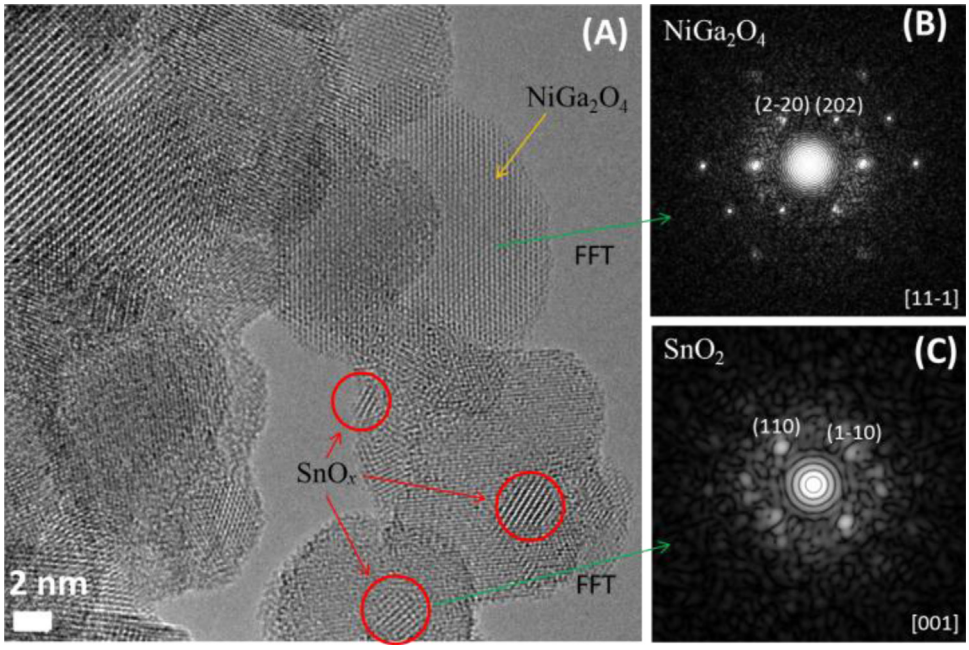

Fig. 2. (A) HRTEM image of SNG 8 composites photocatalyst, the FFT patterns of (B) $NiGa_2O_4$ and (C) SnO_x.

ferent concentration of $SnCl_2$ in 0.1 M HCl) maintained at 353 K in an oil bath and then stirred for a couple of hours. The prepared samples are listed in Table 1. The precipitates were obtained after centrifugal separation and subsequent washing with DI water. The obtained wet precipitate was dried overnight at 353 K.

Yellow SnO_x nano-materials were synthesized by the same procedure described above but without adding $NiGa_2O_4$ particles to the synthesis solution. White rutile SnO_2 was prepared utilizing the above procedure but using $SnCl_4$ as the precursor. SnO was synthesized by previou report [42]. Typically, 2.257 g of $SnCl_2{\cdot}2H_2O$ and 1.612 g of NaOH were put into 20 mL of deionized water in a beaker of 50 mL capacity. After vigorous stirring for 5 min, a black precipitate was obtained. The products were collected by centrifugation, washed three times with de-ionized water and absolute ethanol, respectively, and then dried at 50 °C, the black powders were obtained.

2.2. Materials characterization

The crystal structure was determined by a Bruker D8 focus Powder X-ray diffractometer (XRD) with Cu–Kα radiation (λ = 1.5418 Å) in the 2θ range of 10–80°. Transmission electron microscopy (TEM) images and EDS elemental mapping were collected on a FEI Cs-corrected Titan 80–300 kV microscope with an accelerating voltage of 300 kV. Scanning electron microscopy (SEM) was used a field-emission scanning electron microscope (Hitachi S-4300). UV–vis diffuse reflectance spectra (DRS) were obtained on a Hitachi UV-3010 spectrophotometer using $BaSO_4$ as a ref-

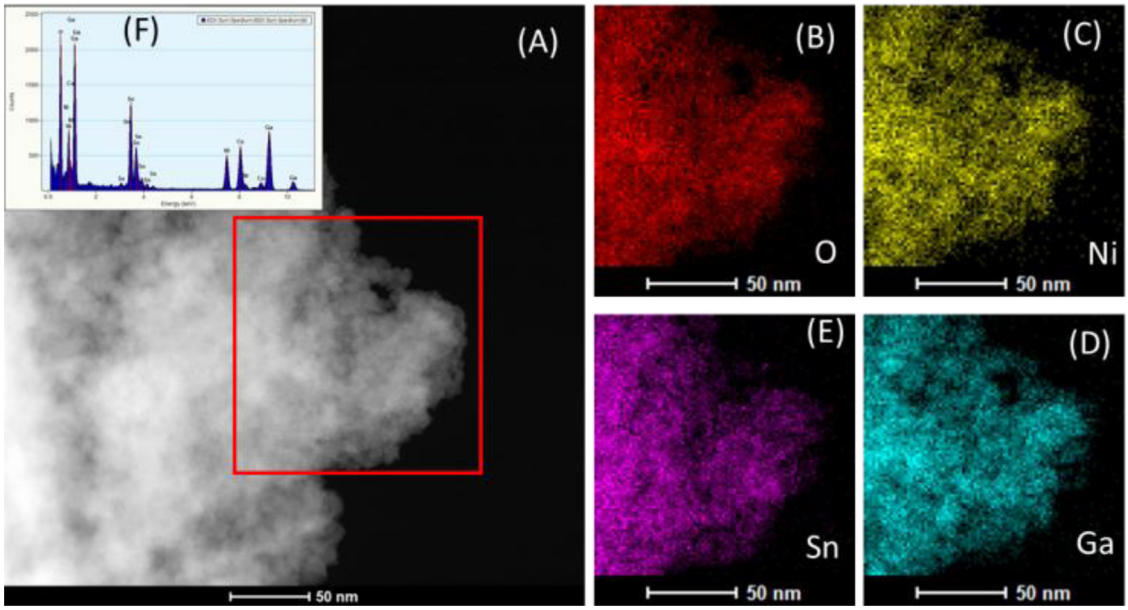

Fig. 3. (A) HAADF-STEM image of SnO_x–$NiGa_2O_4$ materials; (B–E) EDS elemental mapping of the composites, showing uniform distribution of O (B), Ni (C), Ga (D), Sn (E); (F) EDS spectrum of the composites.

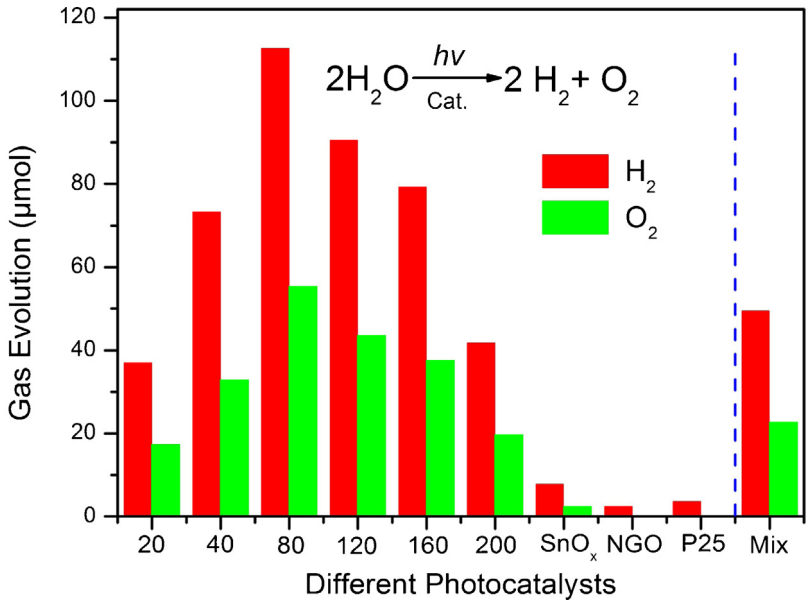

Fig. 4. Specific H_2 and O_2 evolution activities of SNG composites photocatalysts with different SnO_x content. (1) SNG 2 ($y = 20$), (2) SNG 4 ($y = 40$), (3) SNG 8 ($y = 80$), (4) SNG 12 ($y = 120$), (5) SNG 16 ($y = 160$), (6) SNG 20 ($y = 200$), (7) SnO_x, (8) pure $NiGa_2O_4$, (9) P25, (10) mechanically mixed with SnO_x and $NiGa_2O_4$ (the content of Sn equal to $y = 80$). For the photocatalytic experiments, photocatalysts (60 mg) without other cocatalyst were dispersed in deionized water (30 mL) and irradiated with a 300 W high press mercury lamp for 5 h.

erence. The Brunauer–Emmett–Teller (BET) surface areas were measured via nitrogen physisorption Quadrasorb SI-MP surface area analyzer. The desorption isotherm was used to determine the pore size distribution using the Barret–Joyner–Halender (BJH) method, assuming a cylindrical pore modal. X-ray photoelectron spectroscopy (XPS) data were obtained with an ESCALab220i-XL electron spectrometer from VG Scientific using 300 W Al K a radiation. The base pressure was about 3×10^{-9} mbar. The binding energies were referenced to the C1s line at 284.8 eV from adventitious carbon. Fluorescence spectral measurements were carried out with a HITACHI F–4500 fluorescence spectrophotometer; all measurements were made using a 250 nm excitation wavelength. Raman spectra were recorded on an inVia-Reflex Raman microprobe with 532 nm laser excitation. Mott–Schottky experiments were carried out on a three-electrode electrochemical setup using 0.3 M sodium sulfate solution as electrolyte. The SNG electrodes, platinum electrode and saturated calomel electrode (SCE) were used as working electrode, counter electrode and reference electrode, respectively.

2.3. Photocatalytic activity evaluation

Overall water splitting was carried out in a 50 mL quartz tube containing 60 mg photocatalyst in 30 mL pure water. Hydrogen evolution was carried out in a 50 mL quartz tube containing 60 mg photocatalyst in water and methanol solution (30 mL, v/v = 2: 1). The quartz tube was sealed with a rubber septum and degassed by bubbling N_2 through the solution for 30 min at atmospheric pressure. Then the mixture was irradiated by a 300 W high pressure Hg lamp (UV–vis light irradiation). All of the experiments were conducted at room temperature with distilled water. The hydrogen generated from the systems was measured by gas chromatography (GC-14C, Shimadzu Co.) which was equipped with a column (3m × 2 mm) of 5 Å molecular sieves, a thermal conductivity detector and nitrogen carrier gas. The amount of hydrogen and oxygen evolution was calculated versus the external standard method. The cyclic stability tests of the photocatalysts were carried out by opening the sealed cuvette to release the hydrogen after every cycle, the cuvette containing the solution was then subjected to N_2 bubbling for 40 min after which sealed with a rubber septum for photocatalytic reaction again.

The measurements of the amount of •OH were conducted according to the literature [43]. 60 mg of SNG ($y = 80$) photocatalysts were suspended in 50 mL of aqueous solution containing 10 mM NaOH and 3 mM terephthalic acid. Before exposure to visible light irradiation ($\lambda \geq 400$), the suspension was stirred in the dark for 30 min. Then, 5 mL of the solution was taken out every 15 min and centrifuged for fluorescence spectrum measurements. The hydroxyl radicals generated in the presence of the catalyst under visible light irradiation react with the terephthalic acid in solution to form 2-hydroxy terephthalic acid. As it is known that under these low concentrations of terephthalic acid, the hydroxylation proceeds only by the attack of OH• [36]. This molecule has a photoluminescence band at 425 nm and the relative concentration of hydroxyl radicals was then followed by analyzing its intensity using a HITACHI F–4500 fluorescence spectrophotometer.

2.4. Photocurrent measurements

The film electrodes of SnO_x–$NiGa_2O_4$ for the photoelectrochemical response measurements were firstly fabricated. The powders and the ethanol containing Nafion solution (20 mL, 2 wt%) were mixed homogeneously (150 mg/mL), and the obtained paste was then spred on the conducting fluorine—doped SnO_2 glass substrate (FTO, 15 Ω/square) with a glass rod, using adhesive tapes as spacers. Finally, the resultant films have a ca. 4 μm thickness and 1 cm^2 active area. Photocurrent response spectra were measured in a two-electrode configuration, where the $NiGa_2O_4$ photoanodes served as the working electrode with an active area about 1 cm^2 and a platinum wire was used as the counter electrode. The generated photocurrent signals were collected on computer controlled CHI660C electrochemical workstation. A 500-W Xe lamp with a monochromat or and a cutoff filter was used as the light source. The electrolyte was 0.1 M KNO_3 aqueous solution.

3. Results

3.1. Morphology and structure characterization of SNG composites

The physical properties of the SnO_x–$NiGa_2O_4$ composite photocatalysts are shown in Table 1. XRD patterns show that the crystal structure of SNG composites photocatalysts with different content SnO_x obtained from hydrothermal synthesis. Fig. 1A shows that new broad reflections (for example, at ~26.5 2θ in Fig. 1A) were observed after the reaction of nickel gallate with tin precursors, which demonstrated the presence of SnO_x in composites. In addition, the absence of any peak shifts of XRD peak positions of $NiGa_2O_4$ rules out tin incorporation into the structure of $NiGa_2O_4$. This is as expected because the ionic radius of Sn^{2+} is larger than that of Ni^{2+} and Ga^{3+} [36]. And as the content increasing of tin oxide phase, the intensity of the XRD reflections of $NiGa_2O_4$ decreased, possibly due to the changed nanoparticle sizes of $NiGa_2O_4$ as the increasing of SnO_x in the SNG composites [36]. Fig. 1B shows that the crystallinity of SnO_x is very low compared to the SnO and SnO_2, and the reflections of SnO_x contain clearly mixed peaks both of SnO and SnO_2, respectively, for example, 2-theta around 26° is consistent with SnO_2, and around 33° is consistent with SnO, which demonstrates the presence of Sn^{2+} in the SnO_x.

Fig. 2A shows a high-resolution transmission electron microscopy (HRTEM) image of the SNG 8 composites photocatalyst. As demonstrated by the fast Fourier transform (FFT) analysis (Fig. 2B and C), particles with relatively larger sizes in the image are $NiGa_2O_4$, which are decorated with SnO_x nanoparticles identified by the interplanar spacing (~3.3 Å) corresponding to the d spacing of the (1 1 0) plane, and structural analysis indicates that those particles (enclosed by red circles in Fig. 2A) are more like the rutile SnO_2 phase (JCPDS file no. 88–0287) [44]. And this result is in line with our Raman results that the surface of SNG is dominated by tin oxide surface species (shown in Fig. S1). In addition, the size of SnO_x is observed to be around 2–5 nm from the TEM (Fig. S2) and the HRTEM images (Fig. 2A), as would be expected from the broad peaks in the XRD patterns (Fig. 1A).

In order to examine the chemical distribution of the SnO_x–$NiGa_2O_4$ photocatalyst, EDS elemental mapping was performed in scanning TEM mode because the intensity and spread of the color was proportional to the corresponding element's concentration. Fig. 3A shows a high angle annular dark field STEM image of the sample. The EDS mapping recorded from the rectangle region of Fig. 3A clearly shows a homogeneous distribution of O (red, B), Ni (yellow, C), Ga (blue, D), and Sn (purple, E) elements, which solidly demonstrated that the SnO_x is well dispersed in the $NiGa_2O_4$. In addition, EDS spectrum of the sample also confirms that there is only Sn, Ni, Ga elements in the SnO_x–$NiGa_2O_4$ composites, without other impurity found, as shown the insert Fig. 3F and the magnifying EDS (Fig. S3).

3.2. Photocatalytic activity of overall water splitting

The photocatalytic overall water splitting reactions were carried out on the SnO_x–$NiGa_2O_4$ composites photocatalysts with different SnO_x content under UV–vis light irradiation. As shown in Fig. 4, the photocatalytic reaction activities demonstrates that all of these SnO_x–$NiGa_2O_4$ photocatalysts can split overall water into H_2 and O_2 in a ratio of approximately 2:1. And the different content of SnO_x in composites clearly affect the photocatalytic overall water splitting activity. Fig. 4 shows that pure $NiGa_2O_4$ and SnO_x also display very low photocatalytic overall water splitting activity, respectively, as enhancing the y value from 20 to 80, the photocatalytic activity of SNG is also promoted. The photocatalytic activity would gradually decrease when further enhancing the content of SnO_x.

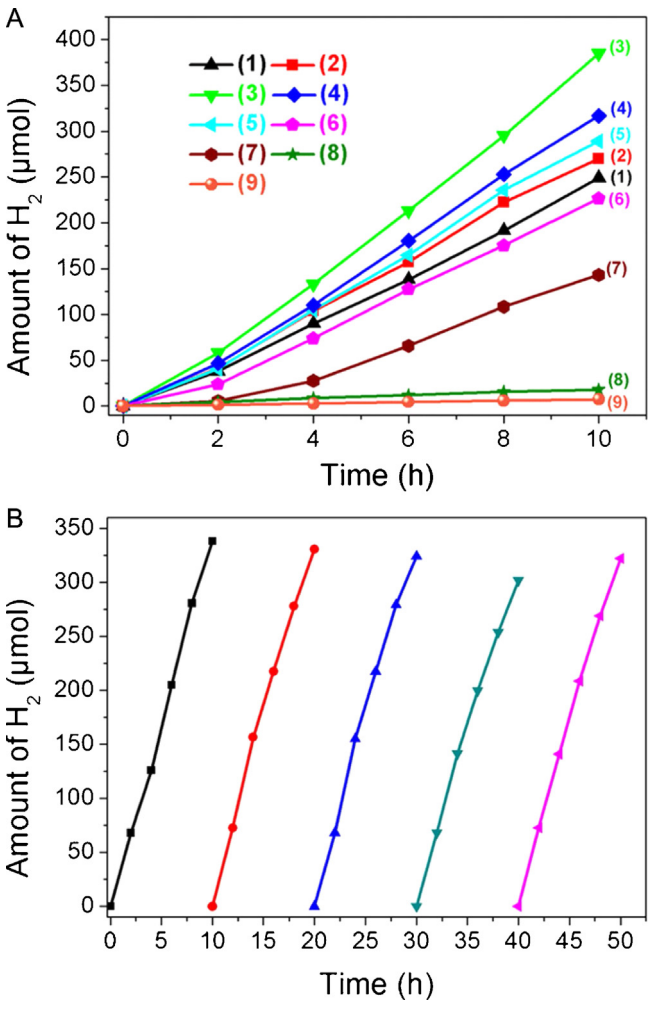

Fig. 5. (A) Specific H_2 evolution activities of SNG composites photocatalysts with different SnO_x content. (1) SNG 2, (2) SNG 4, (3) SNG 8, (4) SNG 12, (5) SNG 16, (6) SNG 20, (7) SnO_x, (8) P25, (9) pure $NiGa_2O_4$. For the photocatalytic reaction experiments, photocatalysts (60 mg) without other cocatalyst were dispersed in deionized water and methanol mixed solution 30 mL (v:v = 2:1) and irradiated with a 300 W high press mercury lamp. (B) Hydrogen evolution activity of SNG 8 photocatalysts for H_2 evolution using methanol aqueous solution under UV–vis light from a 300 W high pressure Hg lamp.

Therefore, the balance of content of SnO_x in SNG composites is very important, the low or high content of SnO_x will not effectively increase the separation of electron–hole of both $NiGa_2O_4$ and SnO_x, corresponding to the low photocatalytic activity. Typically, the photocatalytic activity of composites photocatalysts (SNG 8) reaches up to seven-fold greater than that of $NiGa_2O_4$ or SnO_x alone, respectively. And composites photocatalysts show better photocatalytic water splitting activity compared to TiO_2 (P25) photocatalyst without co-catalyst, which demonstrated the better charge separation of composites photocatalyts than TiO_2. Furthermore, the photocatalytic activity of heterogeneous structure is also higher compared to that of physical mixture of $NiGa_2O_4$ and SnO_x, which means the more effective charge separation of heterostructure photocatalysts. The existence of an optimal SnO_x concentration in the incorporated photocatalysts was primarily due to the balance of an increase in trapping sites leading to efficient trapping and fewer trapped carriers leading to longer lifetimes for interfacial charge transfer [45,46].

In order to demonstrate the effective separation both of photoexcited electrons and holes in SNG composites photocatalysts, the half reaction of hydrogen evolution activity of the SNG composite photocatalysts with different SnO_x content was investigated

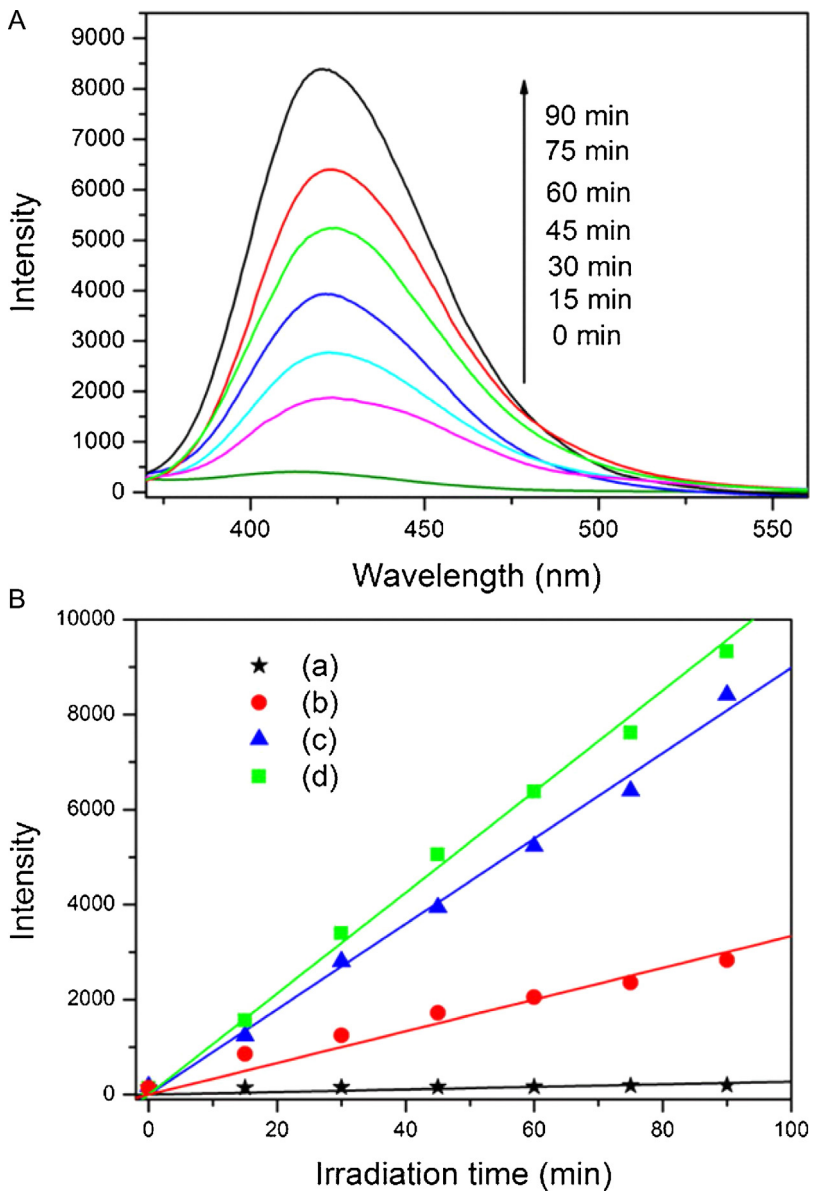

Fig. 6. (A) The fluorescence intensity of 2-hydroxy terephthalic acid using SNG 8 composites, (B) Comparison of time dependence of fluorescence intensity of 2-hydroxy terephthalic acid at 425 nm using (a) without catalysts, (b) $NiGa_2O_4$, (c) SnO_x, (d) SNG 8 under visible light irradiation ($\lambda \geq 400$).

in methanol aqueous solution. In Fig. 5A the SNG shows the similar photocatalytic activity with overall water splitting and demonstrates also that the SnO_x content has a great effect on hydrogen evolution activity in methanol solution. As the SnO_x content increasing, the hydrogen evolution enhances dramatically from 245.5 μmol ($y = 20$) to a maximum of 392.9 μmol ($y = 80$). A further increase of SnO_x content repressed the photocatalytic hydrogen evolution activity of composite photocatalyst. However, $NiGa_2O_4$ or SnO_x alone shows poor photocatalytic hydrogen evolution, and the activity of SNG 8 can also read up to the tens of times greater compared to pure $NiGa_2O_4$ photocatalyst. After deposited 1% Pt, the SNG composites show better photocatalytic activity (shown in Fig. S4). And the SNG composites photocatalysts show better photocatalytic hydrogen evolution activity compared to SnO_x–$ZnGa_2O_4$ and SnO_x–$ZnGe_2O_4$ composites photocatalysts (Fig. S5), which indicates the better photocatalytic potential of SNG. As SNG 8 composites photocatalysts show the optimum hydrogen production, the hydrogen-evolution stability of the SNG 8 was investigated in aqueous solution using methanol as a sacrificial electron donor (Fig. 5B). The results showed the robust hydrogen evolution activity of the photocatalysts with almost no decrease after 5 cycles of photocatalytic irradiation for a period of 50 h, which solidly demonstrates the photochemical stability of SnO_x and $NiGa_2O_4$ heterostructure with the well-junction.

The effective separation of electron and hole can prolong the lifetime of electron and hole, which is likely responsible for enhancing the photocatalytic activity. However, it is impossible for all of the long-lived charge carriers to have the opportunity to reach the surface of the photocatalysts and participate in the course of surface redox reaction [15]. The fluorescence intensity of 2-hydroxy terephthalic acid can be used to detect the oxidation capability of holes via the formation of hydroxyl $OH^•$ radicals by reaction of holes with surface hydroxyl groups or physisorbed water molecules at the surface of composites photocatalysts [43]. Here, we used the formation of more hydroxyl $OH^•$ radicals to illustrate that the charges and holes can be separated and with large holes emigrated to the surface of semiconductor (as shown in Fig. 6A). Fig. 6B clearly shows that composites photocatalyst could form more hydroxyl

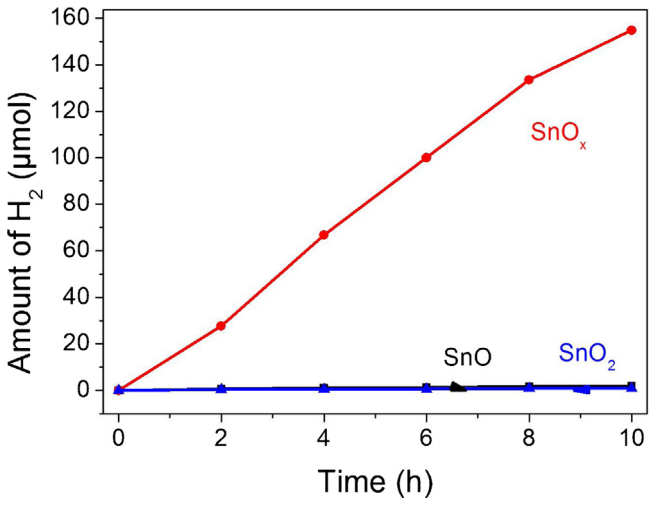

Fig. 7. The photocatalytic hydrogen evolution by different SnO, SnO_2 and SnO_x photocatalysts without any cocatalytst in methanol aqueous solution under UV–vis light from a 300 W high pressure Hg lamp.

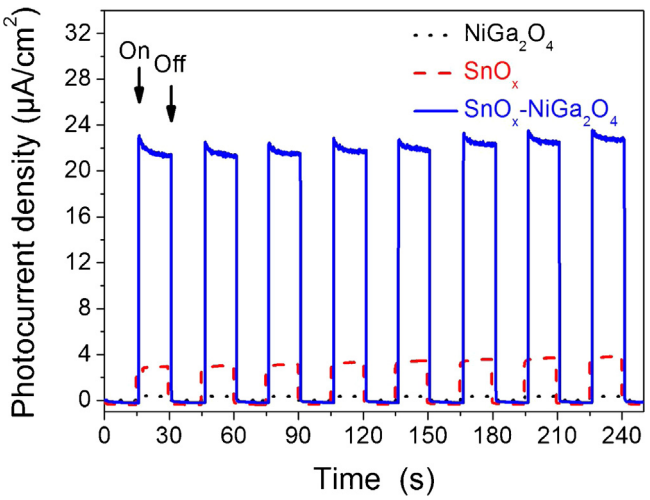

Fig. 8. The on–off photocurrent (I–t) without bias in a two-electrode configuration for the (1) $NiGa_2O_4$ (dot), (2) SnO_x (shot line), (3) SNG 8 composites (line) as photoanodes, in 0.1 M KNO_3 solution, respectively.

OH• radicals with the increasing of illumination time, and the fluorescence intensity is clearly stronger than the SnO_x and $NiGa_2O_4$, respectively, which means that the SnO_x–$NiGa_2O_4$ photocatalyst has better charge separation, and large holes can reach the surface of photocatalysts, consequently resulting in better photocatalytic water splitting activity. The forming of larger hydroxyl OH• radicals also demonstrated that the SNG composites have the excellent potential for applications in remediation of the organic pollution under the visible irradiation, for example the photodegradation of methylene blue or cresol etc.

4. Discussions

4.1. The roles of SnO_x for enhancing photocatalytic activity

Recently, nonstoichiometric metal oxides (self-doped) without introducing impurity elements have been developed and demonstrated to be one effective method to make the semiconductor sensitive to visible light [47–50]. Such as a high concentration of Ti^{3+} could generate a continuous vacancy-induced band of electronic states below the conduction band of TiO_2, and these states facilitate the transport of the photocarriers to the active sites on the surface, which would be responsible for the enhancement of the photocatalytic activity [50]. Self-doped perovskite structure $SrTiO_3$-δ also shows that oxygen deficiency can improve the chemical adsorption of CO_2 and accommodate CO_2 molecule in the oxygen vacancy, thereby, the synergetic effect of visible light absorption and chemical adsorption of CO_2 can effectively improve the artificial photosynthesis to generate hydrocarbon fuels from CO_2/H_2O [48]. Sn^{2+} self-doped SnO_{2-x} has been demonstrated to show exceptionally higher visible-light photocatalytic activity than stoichiometric SnO_2, which is ascribed to the incorporation of Sn^{2+} into the lattice matrix and accompanying oxygen vacancies, resulting in narrowing the band gap and efficient separation of the photoexcited electron–hole pairs [34,51]. And more important, SnO_x have better photocatalytic hydrogen evolution activity compared to alone SnO or SnO_2 photocatalyst (as shown in Fig. 7) under the UV–vis light irradiation, which is attributed to the desirable band structure and effective charge separation for photocatalytic H_2 evolution from aqueous solution, which originates from the coexistence of Sn^{2+} and Sn^{4+} in SnO_x [52]. Therefore, SnO_x combined with other semiconductors would exhibit greater enhancement in photocatalytic activity.

4.2. Photoelectrochemical ability for the recombination of photo-excited electon-hole pair

Photoelectrochemical measurement is an effective method to verify the separation of photo-excited charge carrier in semiconductors and to demonstrate that the electron and hole pair can efficiently emigrate to the surface of semiconductors. Fig. 8 shows that the SNG 8 photocatalysts display the best photo-excited current and the photocurrent can reach up to 8 times compared to SnO_x electrode, and pure $NiGa_2O_4$ shows the smallest photocurrent, which indicated a much more efficient charge separation for the SNG 8 photocatalysts. The photoelectrochemical experiment results are well consistent with the photocatalytic activity results. In addition, the photoelectrochemical results also show the well stability of photoexcited current after 8 cycles of turn on—off light irradiation, which also demonstrated the good photo-stability of SNG 8 photocatalysts. Furthermore, the photoluminescence spectroscopy experiments (shown in Fig. S6) also demonstrated that the electrons from the conduction band of $NiGa_2O_4$ can be injected into the conduction band of SnO_x, resulting in enhancing of the electron–hole separation. The effective separation of charge are most likely responsible for the enhancement in the photocatalytic activity of SNG [15].

4.3. The mechanistic insight of charge transfer between SnO_x and $NiGa_2O_4$

Photocatalytic overall water splitting and hydrogen evolution experiments demonstrated the better photocatalytic activity of SNG composites, which is attributed to the effective charge separation between SnO_x and $NiGa_2O_4$. The band gap structures of $NiGa_2O_4$ and SnO_x were examined and further used to demonstrate the charge separation mechanism by XPS, DRS and Mott–Schottky measurements. From the Fig. 9A we can see that the value band edge of SnO_x (2.6 eV) is clearly more positive compared to the $NiGa_2O_4$ (1.25 eV), and with the enhancement of SnO_x content, the value band edge of SnO_x–$NiGa_2O_4$ clearly exhibited positive shift, which also demonstrated the effect of SnO_x on the $NiGa_2O_4$. We also see that the valence band edge of SnO_2 was 3.21 eV, which is more positive than that of SnO_x (2.6 eV), verifying that Sn^{2+} will increase the value band edge and reduce the band gap of SnO_2, which is attributed to that the Sn^{2+} could generate a continuous vacancy band of electronic states below the conduction band of SnO_2 [50],

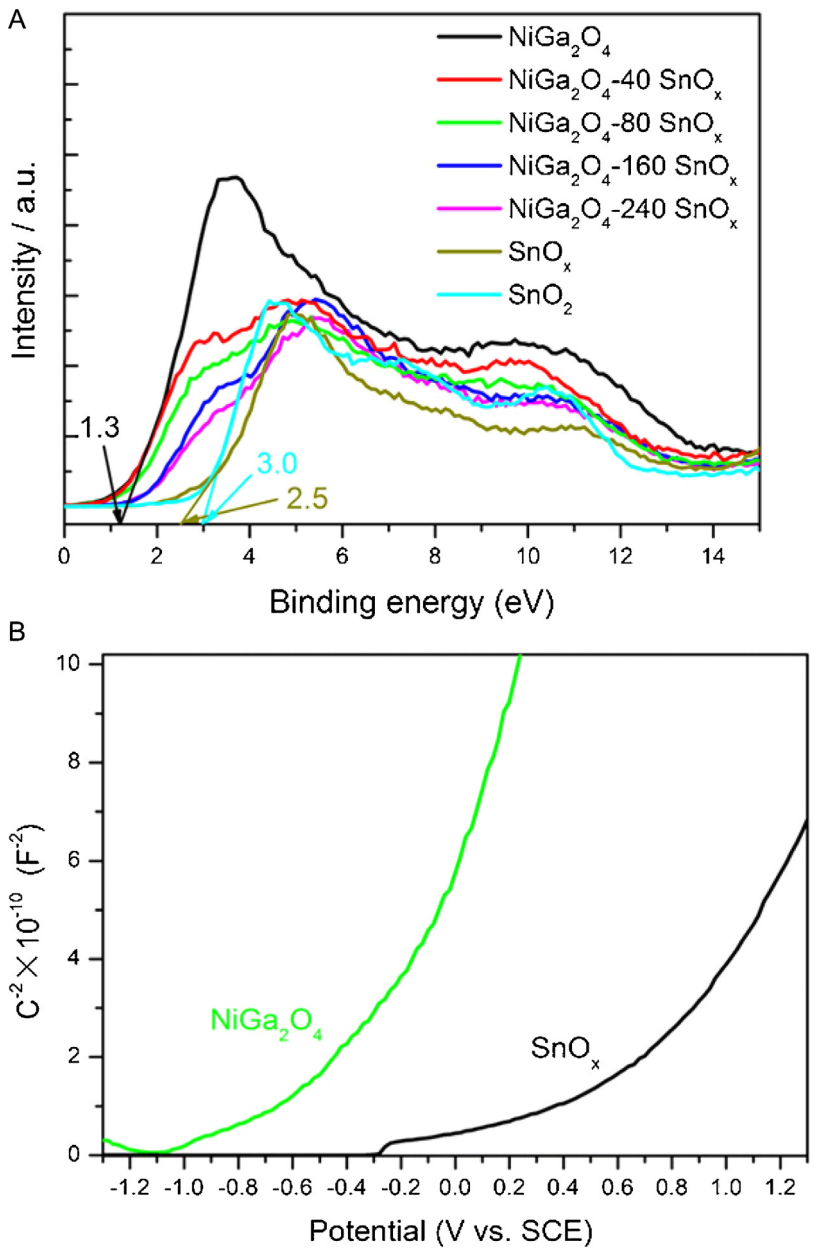

Fig. 9. (A) The valence band spectra of the SnO_x–$NiGa_2O_4$ with different SnO_x content, alone SnO_x and SnO_2 photocatalysts. SnO_x and SnO_2 photocatalysts. (B) Mott–Schottky curves of $NiGa_2O_4$ and SnO_x electrodes measured in Na_2SO_4 solution (0.3 M, pH Ca. 7.0).

and the Sn^{2+} doping would also increase oxygen vacancies and enhance the light harvesting [34]. Furthermore, the Mott–Schottky measurement also shows that the flat band potential of $NiGa_2O_4$ is more negative than that of SnO_x (Fig. 9B), which is coincident with the calculation based on the valence band spectra and the band gap, and more importantly demonstrates the possibility of electron transfer from the conduction band of $NiGa_2O_4$ to that of SnO_x. Fig. S7 shows that the band gaps of $NiGa_2O_4$ and SnO_x are 3.54 eV and 2.8 eV, respectively. In addition, the absorption edge of SnO_x is intermediate between SnO_2 and SnO (Fig. S7C, D), and exhibit a broad range of absorption of visible light in the absorption spectrum in the UV/vis range. The synthesized SnO material is black nanoparticles and exhibits no distinct absorption edge, suggesting that SnO is either a narrow-gap semiconductor or a semimetal [52]. The SnO_2 had clear UV region absorption, whereas the SnO_x material had orange color and showed the visible absorption trailing, a narrower band gap (2.8 eV) than that of SnO_2 (3.5 eV). The red shift of SnO_x was attributed to the presence of Sn^{2+} in the composites, and the contribution of Sn 5s orbitals to the valence band formation [53].

Based on the static data discussion of the valence band potential edge by means of XPS, DRS, and Mott–Schottky measurements, the band gap and further taking into account the flat band potential between the two semiconductors, we draw the band structure scheme of photoexcited electron–hole pairs (as shown in Fig. 10), and the electrons will tend to transfer from the semiconductor $NiGa_2O_4$ to that of SnO_x, while the photoexcited holes in the value band of SnO_x will transfer simultaneously to the valence band of $NiGa_2O_4$, which also demonstrate the pollution degradation potential of the SnO_x–$NiGa_2O_4$ photocatalysts under visible light irradiation via hole transfer from SnO_x to the valence band of $NiGa_2O_4$. Consequently, the transfer between two semiconductors will effectively suppress the recombination of charge

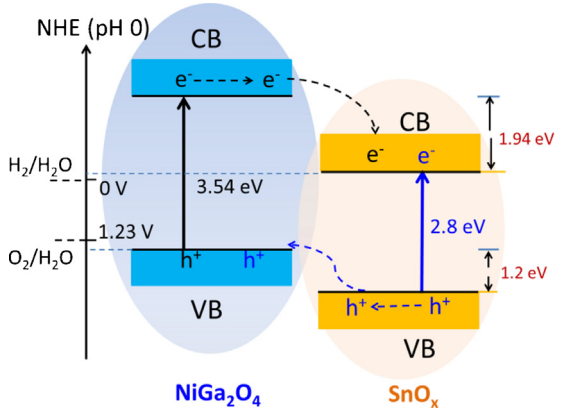

Fig. 10. Illustration of photo-excited charge separation and transfer between the two semiconductors.

photogeneration in semiconductor, which enhances the photocatalytic overall water splitting activity.

5. Conclusions

We applied the SnO_x as the surface species and combined with $NiGa_2O_4$ to form a composite photocatalysts for the first time. Owing to the efficient charge separation and transfer between the SnO_x and $NiGa_2O_4$, the synthesized composites exhibited a remarkably enhanced photocatalytic overall water splitting activity compared to those of SnO_x–$ZnGa_2O_4$, $NiGa_2O_4$ and SnO_x photocatalysts, respectively. Furthermore, we elucidated the essential relation between the photocatalytic activity and the structure of photocatalyst, and studied in depth the mechanism of effective separation of charge based on the band alignment in this system. Our work is expected to provide some insight in the design and preparation of efficient semiconductor based photocatalysts.

Acknowledgements

This work was financially supported by the National Key Basic Research Program of China (973 Program 2013CB834804) and the Ministry of Science and Technology (2012DFH40090). We thank the Natural Science Foundation of China (21107117, 21353002, 21477136), Beijing Natural Science Foundation (2132057) for financial support. We also appreciate the TEM support from the Fritz Haber Institute of Max Planck Society.

Appendix A. Supplementary data

Supplementary data associated with this article can be found, in the online version, at http://dx.doi.org/10.1016/j.apcatb.2015.09.032.

References

[1] K. Maeda, K. Teramura, D. Lu, T. Takata, N. Saito, Y. Inoue, K. Domen, Nature 440 (2006) 295.
[2] T. Ohno, L. Bai, T. Hisatomi, K. Maeda, K. Domen, J. Am. Chem. Soc. 134 (2012) 8254–8259.
[3] C. Liu, J. Tang, H.M. Chen, B. Liu, P. Yang, Nano Lett. 13 (2013) 2989–2992.
[4] P.D. Tran, L.H. Wong, J. Barber, J.S.C. Loo, Energy Environ. Sci. 5 (2012) 5902–5918.
[5] A. Kubacka, M. Fernández-García, G. Colón, Chem. Rev. 112 (2012) 1555–1614.
[6] X. Chen, S. Shen, L. Guo, S.S. Mao, Chem. Rev. 110 (2010) 6503–6570.
[7] M.G. Walter, E.L. Warren, J.R. McKone, S.W. Boettcher, Q. Mi, E.A. Santori, N.S. Lewis, Chem. Rev. 110 (2010) 6446–6473.
[8] N. Serpone, A.V. Emeline, J. Phys. Chem. Lett. 3 (2012) 673–677.
[9] K. Maeda, K. Domen, J. Phys. Chem. Lett. 1 (2010) 2655–2661.
[10] T.W. Kim, K.S. Choi, Science 343 (2014) 990–994.
[11] Y. Sasaki, H. Kato, A. Kudo, J. Am. Chem. Soc. 135 (2013) 5441–5449.
[12] H. Kato, K. Asakura, A. Kudo, J. Am. Chem. Soc. 125 (2003) 3082–3089.
[13] T.K. Townsend, N.D. Browning, F.E. Osterloh, Energy Environ. Sci. 5 (2012) 9543–9550.
[14] A. Kudo, Y. Miseki, Chem. Soc. Rev. 38 (2009) 253–278.
[15] X. Wang, Q. Xu, M. Li, S. Shen, X. Wang, Y. Wang, Z. Feng, J. Shi, H. Han, C. Li, Angew. Chem. Int. Ed. 51 (2012) 13089–13092.
[16] K. Maeda, A. Xiong, T. Yoshinaga, T. Ikeda, N. Sakamoto, T. Hisatomi, M. Takashima, D. Lu, M. Kanehara, T. Setoyama, T. Teranishi, K. Domen, Angew. Chem. Int. Ed. 49 (2010) 4096–4099.
[17] C. Cheng, A. Amini, C. Zhu, Z.L. Xu, H.S. Song, N. Wang, Sci. Rep. 4 (2014) 4181.
[18] J. Yang, D. Wang, H. Han, C. Li, Acc. Chem. Res. 46 (2013) 1900–1909.
[19] X.J. Lv, W.F. Fu, H.X. Chang, H. Zhang, J.S. Cheng, G.J. Zhang, Y. Song, C.Y. Hu, J.H. Li, J. Mater. Chem. 22 (2012) 1539–1546.
[20] J. Tian, Y. Sang, Z. Zhao, W. Zhou, D. Wang, X. Kang, H. Liu, J. Wang, S. Chen, H. Cai, H. Huang, Small 9 (2013) 3864–3872.
[21] M. Zhong, Y. Li, I. Yamada, J.-J. Delaunay, Nanoscale 4 (2012) 1509–1514.
[22] S. Balachandran, M. Swaminathan, J. Phys. Chem. C 116 (2012) 26306–26312.
[23] M.T. Uddin, Y. Nicolas, C. Olivier, T. Toupance, L. Servant, M.M. Müller, H.J. Kleebe, J. Ziegler, W. Jaegermann, Inorg. Chem. 51 (2012) 7764–7773.
[24] K. Vinodgopal, I. Bedja, P.V. Kamat, Chem. Mater. 8 (1996) 2180–2187.
[25] C.Y. Lin, Y.H. Lai, D. Mersch, E. Reisner, Chem. Sci. 3 (2012) 3482–3487.
[26] W. Wang, X. Huang, S. Wu, Y. Zhou, L. Wang, H. Shi, Y. Liang, B. Zou, Appl. Catal. B: Environ. 134 (2013) 293–301.
[27] W. Zhou, C. Cheng, J. Liu, Y.Y. Tay, J. Jiang, X. Jia, J. Zhang, H. Gong, H.H. Hng, T. Yu, H.J. Fan, Adv. Funct. Mater. 21 (2011) 2439–2445.
[28] H. Tada, Q. Jin, H. Nishijima, H. Yamamoto, M. Fujishima, S. i. Okuoka, T. Hattori, Y. Sumida, H. Kobayashi, Angew. Chem. Int. Ed. 50 (2011) 3501–3505.
[29] A.M. Hussein, R.V. Shende, Int. J. Hydrog. Energy 39 (2014) 5557–5568.
[30] T. Giannakopoulou, N. Todorova, M. Giannouri, J. Yu, C. Trapalis, Catal. Today 230 (2014) 174–180.
[31] C. Cheng, H. Zhang, W. Ren, W. Dong, Y. Sun, Nano Energy 2 (2013) 779–786.
[32] Q. Jin, M. Fujishima, M. Nolan, A. Iwaszuk, H. Tada, J. Phys. Chem. C 116 (2012) 12621–12626.
[33] U.V. Desai, C. Xu, J. Wu, D. Gao, J. Phys. Chem. C 117 (2013) 3232–3239.
[34] C.M. Fan, Y. Peng, Q. Zhu, L. Lin, R.X. Wang, A.W. Xu, J. Phys. Chem. C 117 (2013) 24157–24166.
[35] W.P. Zhou, W. An, D. Su, R. Palomino, P. Liu, M.G. White, R.R. Adzic, J. Phys. Chem. Lett. 3 (2012) 3286–3290.
[36] V.B.R. Boppana, R.F. Lobo, ACS Catal. 1 (2011) 923–928.
[37] J. Shi, W. Yu, I. Bergmann, H. Bremers, V. Šepelák, W. Mader, K.D. Becker, J. Alloy. Compd. 504 (2010) S432–S434.
[38] H. Xue, Z. Li, Z. Ding, L. Wu, X. Wang, X. Fu, Cryst. Growth Des. 8 (2008) 4511–4516.
[39] L. Chen, T. Horiuchi, T. Mori, Appl. Catal. A: Gen. 209 (2001) 97–105.
[40] S.X. Zhou, X.J. Lv, C. Zhang, X. Huang, L. Kang, Z.S. Lin, Y. Chen, W.F. Fu, ChemPlusChem 80 (2015) 223–230.
[41] S.C. Yan, S.X. Ouyang, J. Gao, M. Yang, J.Y. Feng, X.X. Fan, L.J. Wan, Z.S. Li, J.H. Ye, Y. Zhou, Z.G. Zou, Angew. Chem. Int. Ed. 49 (2010) 6400–6404.
[42] B. Liu, J. Ma, H. Zhao, Y. Chen, H. Yang, Appl. Phys. A: Mater. 107 (2012) 437–443.
[43] Z. Chen, D. Pan, Z. Li, Z. Jiao, M. Wu, C.H. Shek, C.M. Wu, J.K. Lai, Chem. Rev. 114 (2014) 7442–7486.
[44] S. Xu, D.D. Sun, Int. J. Hydrog. Energy 34 (2009) 6096–6104.
[45] X.J. Lv, S.X. Zhou, C. Zhang, H.X. Chang, Y. Chen, W.F. Fu, J. Mater. Chem. 22 (2012) 18542–18549.
[46] G. Liu, L. Wang, C. Sun, X. Yan, X. Wang, Z. Chen, S.C. Smith, H.M. Cheng, G.Q. Lu, Chem. Mater. 21 (2009) 1266–1274.
[47] X. Xu, C. Randorn, P. Efstathiou, J.T.S. Irvine, Nat. Mater. 11 (2012) 595–598.
[48] K. Xie, N. Umezawa, N. Zhang, P. Reunchan, Y. Zhang, J. Ye, Energy Environ. Sci. 4 (2011) 4211–4219.
[49] M. Choi, F. Oba, Y. Kumagai, I. Tanaka, Adv. Mater. 25 (2013) 86–90.
[50] I. Justicia, P. Ordejón, G. Canto, J.L. Mozos, J. Fraxedas, G.A. Battiston, R. Gerbasi, A. Figueras, Adv. Mater. 14 (2002) 1399–1402.
[51] W.P. Zhou, S. Axnanda, M.G. White, R.R. Adzic, J. Hrbek, J. Phys. Chem. C 115 (2011) 16467–16473.
[52] M. Manikandan, T. Tanabe, P. Li, S. Ueda, G.V. Ramesh, R. Kodiyath, J. Wang, T. Hara, A. Dakshanamoorthy, S. Ishihara, K. Ariga, J. Ye, N. Umezawa, H. Abe, ACS Appl. Mater. Interface 6 (2014) 3790–3793.
[53] Y. Hosogi, Y. Shimodaira, H. Kato, H. Kobayashi, A. Kudo, Chem. Mater. 20 (2008) 1299–1307.